JOINT EUROPEAN TORUS

JET–P(86)46

D.J. Campbell, J.P. Christiansen, J.G. Cordey, E. Lazzaro,
M.F.F. Nave, F.C. Schueller and P.R. Thomas

Current and Temperature Profile Evolution in JET

Current and Temperature Profile Evolution in JET

D.J. Campbell, J.P. Christiansen, J.G. Cordey, E. Lazzaro,
M.F.F. Nave, F.C. Schueller and P.R. Thomas

JET-Joint Undertaking, Culham Science Centre, OX14 3DB, Abingdon, UK

Preprint of Paper to be submitted for publication in
Nuclear Fusion

CURRENT AND TEMPERATURE PROFILE EVOLUTION IN JET

D.J. Campbell, J.P. Christiansen, J.G. Cordey, E. Lazzaro,
M.F.F. Nave, F.C. Schueller and P.R. Thomas

JET Joint Undertaking, Abingdon, Oxon. OX14 3EA, U.K.

ABSTRACT

The evolution of the current and temperature profiles in JET has been analysed using current profiles derived from advanced equilibrium analysis codes, and temperature profiles obtained from absolutely calibrated ECE measurements. It is found that current evolution during the discharge 'flat-top' is well described by neoclassical, rather than Spitzer, resistivity. During the current rise phase however, current penetration is substantially more rapid than expected. The mhd processes influencing the rapid penetration are discussed, and a new analysis of this mhd activity based on the trajectories of discharges in the (q_o, q_a) plane is presented.

1. INTRODUCTION

The identification of processes influencing the formation of the current profile in a tokamak is important both at the practical operational level, and at the fundamental level of understanding basic transport mechanisms and regimes. Here an analysis of tokamak temperature and current profiles is presented in which the temporal evolution of these profiles is studied for a large number of plasma discharges in JET (R_o = 2.96m, a < 1.25m, b/a < 1.6, I_p < 5MA, B_ϕ < 3.45T). The principal diagnostics used are the equilibrium identification codes IDENTC and FAST [1-2], which make use of external magnetic measurements to calculate parametrised current density profiles, and an absolutely calibrated ECE diagnostic which provides temperature profiles [3].

The process of current penetration in tokamaks has been examined in detail by many authors [4-10], and it has invariably been found that current penetration occurs faster than expected classically. It is generally concluded that the anomalous penetration is due to instabilities which reconnect field lines across the plasma, redistributing current and energy. In LT-3 [5] for example, the rapid peaking of the originally hollow current

profile was associated with the occurrence of an m=4 mode, and was accompanied by a rapid radial diffusion of runaway electrons. A study on Alcator A [6] also observed the occurrence of mhd activity during the current rise phase. An analytic model of the current profile was used to deduce a criterion for a marginally hollow current profile in terms of the central electron temperature. The authors concluded that the disruptive activity observed arose from the formation of hollow current profiles, which occurred in spite of the fact that the temperature profile was always peaked during the discharge rise phase. More recently it has been found in ASDEX [9] and PDX [10] that the level and type of mhd activity observed could be influenced by the rate of current rise. An investigation of current diffusion in Doublet III [8], in which the current was ramped from one steady-state value to a second steady-state, concluded that current diffusion occurred classically for values of the current ramp rate $\dot{I}_p$ up to $7MAs^{-1}$, although disruptions occurred during the transition to the second steady state for values of $\dot{I}_p$ above $2MAs^{-1}$.

The picture which emerges from these experimental investigations is broadly in agreement with theoretical expectations [11-13], in which a hollow current profile can be unstable to 'double-tearing' modes, while a peaked current profile may be unstable to resistive kink modes.

In this paper we present the results of an investigation of current diffusion during several phases of the JET discharge: the current rise phase, the current flat top, and a current ramp between 'steady-state' values. The evolution of the current profile is investigated using the equilibrium identification codes IDENTC and FAST, which provide information on the profiles of current density and plasma resistivity from external magnetic measurements. Resistivity profiles obtained in this way are compared with profiles of Spitzer and neoclassical resistivity calculated from electron temperature profiles deduced from ECE measurements, density profiles from microwave and far-infrared interferometry, and Z_{eff} values calculated from visible bremsstrahlung emission.

We find that the ECE temperature profile measurements obtained during the discharge flat-top are fully consistent with current profiles deduced independently from magnetic signals by the equilibrium codes. We conclude that the plasma resistivity is in general neoclassical during the flat-top. In addition, we find that current diffusion during a current ramp between two steady-states is neoclassical for the ramp rates used ($\dot{I}_p \lesssim 0.5MAs^{-1}$).

During the current rise phase, however, current penetration occurs on a timescale which is much shorter than the neoclassical skin time, from which we deduce that the effective plasma resistivity is enhanced during this period. Furthermore, during the early stage of the discharge substantial mhd activity is observed. The association between this activity and the process of current penetration is investigated by analysing the trajectory of typical discharges in the (q_o, q_a) plane, where q_o is the central value of the field-line q, and q_a the edge value. Superimposing the boundaries of various mhd stability regions, as obtained from the model of [13], in this plane yields an interpretation of the processes accompanying current penetration during the early stage of the discharge.

2. METHOD OF ANALYSIS

2.1 Magnetic Equilibrium Analysis

The "generalised" Ohm's law for an isotropic plasma is:

$$\underline{E} = - \underline{v} \times \underline{B} + \eta_{\parallel} \underline{J}_{\parallel} + \eta_{\perp} \underline{J}_{\perp} + \frac{1}{ne} [\underline{R}_T - \underline{\nabla} p], \qquad (1)$$

where the last term containing the thermal drag force

$$\underline{R}_T = -0.71\ nk\ \nabla_{\parallel} T_e - \frac{3}{2} \frac{nk}{\omega_{ce} \tau_e} \frac{\underline{B}}{B} \times \underline{\nabla}_{\perp} T_e$$

is of the order of the inertial term in the momentum balance equation.

Irrespective of the convective term the parallel resistivity is defined from:

$$\eta_{\parallel} = \underline{E} \cdot \underline{B} / \underline{J} \cdot \underline{B} \ . \qquad (2)$$

Introducing the radial variable $\rho = \sqrt{\frac{\phi}{\pi B_o}}$ related to the toroidal flux ϕ, in conditions of steady toroidal field B_o, we may define an effective parallel resistivity from the equation for the evolution of the poloidal flux ψ, obtaining from the surface averages $\langle \underline{E} \cdot \underline{B} \rangle$ and $\langle \underline{J} \cdot \underline{B} \rangle$

$$\eta_{eff} = \frac{\left.\frac{\partial \psi}{\partial t}\right|_{\rho = \text{const}}}{\frac{\rho}{\mu_0 C_0^2} \frac{\partial}{\partial \rho}\left[\frac{C_0 C_1}{\rho} \frac{\partial \psi}{\partial \rho}\right]}, \qquad (3)$$

where $C_0 = \frac{\partial V}{\partial \rho}\left\langle \frac{1}{R^2} \right\rangle$, $C_1 = \frac{\partial V}{\partial \rho}\left\langle \left(\frac{\nabla \rho}{R}\right)^2 \right\rangle$ and V is the plasma volume.

The averages $\langle A \rangle$ are defined as $\langle A \rangle = \frac{\int_\Gamma A \frac{d\ell}{B_p}}{\int_\Gamma \frac{d\ell}{B_p}}$,

Γ being the plasma contour, and B_p the poloidal field.

The plasma configuration $(\psi(R,z), \Gamma, V)$ is obtained by solving a time sequence of inverse Grad-Shafranov equilibrium problems which fit the flux and tangential magnetic field measurements on the tokamak vessel resulting from a toroidal current density J_ϕ, found suitable for JET:

$$J_\phi(E,\psi) = I_0\left[\alpha \frac{R}{R_0}\left(1-\psi + b(1-\psi)^2\right) + (1-\alpha)\frac{R_0}{R}\left(1-\psi + a(1-\psi)^2\right)\right] \qquad (4)$$

In (4) a,b,α are free parameters which are determined by a fit to the measurements. The fit is based on the search for a minimum (least squares fit) of the χ^2 functional for the tangential magnetic field on the vessel

$$\chi^2 = \left|\left|\frac{1}{R}\frac{\partial \psi}{\partial n} - B^{exp}\right|\right|^2_{\Gamma_{vessel}}, \qquad (5)$$

subject to the constraint that the flux function $\psi(R,z)$ satisfies the equilibrium problem [1]

$$R^2 \nabla \cdot \left(\frac{\nabla \psi}{R^2}\right) = -R\left[RP'(\psi,a,\alpha) + \frac{FF'(a,b,\alpha)}{R}\right]\psi, \qquad (6)$$

and

$$\psi\big|_{\Gamma_{vessel}} = \psi^{exp}.$$

ψ^{exp} and B^{exp} are the experimental measurements and $\frac{\partial\psi}{\partial n}$ is the normal derivative of ψ on the vessel surface.

While one of the parameters (α) is chosen to be compatible with other measurements (i.e. diamagnetic loop measurements), the other two parameters a,b are identified via (5) and allow for the separation of the pressure and paramagnetic flux term in expression (6). The safety factor profile is then obtained as

$$q = -\frac{1}{2\pi}\frac{\partial\phi}{\partial\psi} = -\frac{1}{4\pi^2}\frac{\partial V}{\partial\rho}\left\langle\frac{1}{R^2}\right\rangle F(\psi,b,\alpha) \ . \qquad (7)$$

The effective resistivity given by (3) includes effects of collisional origin as well as effects caused by instabilities. Values of η_{eff} can then be compared with the resistivity derived from the ECE temperature diagnostics.

The penetration time associated with η_{eff} is also influenced by the geometry of the plasma and it is of order

$$\tau = a^2 \frac{\mu_o}{\eta_{eff}} \frac{E^2}{1+E^2}\left(1+\frac{\Delta}{R_o}\right) , \qquad (8)$$

where a,E,Δ are the minor radius, elongation ratio and magnetic axis shift of the plasma; τ can be significantly shorter than the neoclassical estimate (several seconds for JET) whenever instabilities are present.

2.2 Plasma Resistivity

Profiles of 'plasma' resistivity are derived from local parameters obtained by diagnostic measurements. The principal input data are $T_e(r)$ from ECE [3], $n_e(r)$ from microwave or far-infrared interferometry, and $\bar{Z}_{eff}$ from visible Bremsstrahlung measurements. 'Spitzer' parallel resistivity is calculated from:

$$\eta_s = 1.034\times10^{-4}\ Z_{eff}\ \alpha\ (Z_{eff})\ \ell n\ \Lambda_e / T_e^{3/2} \qquad (9)$$

and neoclassical resistivity from:

$$\eta_* = g\eta_S \qquad \text{where } g = (1-f_T/(1+\xi\nu_*))^{-1}(1-C_R f_T/(1+\xi\nu_*))^{-1}. \qquad (10)$$

Explicit forms of the coefficients $\alpha(Z_{eff})$, ξ, C_R, the electron trapping factor f_T, and the collisionality ν_* are given in [14]. The principal sources of error in these calculations arise from the measurement of $T_e(r)$ (±10%), and Z_{eff} (the profile is assumed to be flat).

The evolution of the principal parameters of a pulse selected for analysis is shown in figure 1a, while the evolution of the temperature profile, measured by ECE, during the first 5s of this discharge is shown in figure 1b. The hollow temperature profiles occurring during the first 1.5s are commonly, though not invariably, observed in JET. Note that the plasma is 'grown' from the limiter (at R = 4.2m), so that during the current ramp phase the plasma centre moves from R ~ 3.3m to R ~ 3m. As will be discussed later, during the period in which the temperature profile evolves from hollow to peaked, the current profiles calculated from magnetic equilibrium analysis evolve in the same way. However, it is found that the two profiles are not related by Spitzer or neoclassical resistivity during this time.

This is illustrated in figure 2 which shows a comparison of radial profiles of η_{eff} (crosses), η_S (full line) and η_* (dashed line) at several times during the rise phase and flat top of this discharge. During the first 2s of the plasma there are significant differences between the values of η_{eff} and η_*, and particularly during the first 0.7s, where η_{eff} is significantly higher than η_*. Thus, the current penetration occurs more rapidly than can be explained by neoclassical resistivity. This might be explained by magnetic relaxation, as discussed in section 3. Once the plasma current has reached its equilibrium value however, the profiles of resistivity derived from magnetic analysis (η_{eff}) and from temperature measurements (η_*) are in very good agreement. This point is further emphasised in figure 3, where profiles of η_{eff}, η_S, and η_* are compared for a wide range of conditions in JET with plasma current ranging from 1 to 4MA, and average density from 1 to $2.7\times10^{13}m^{-3}$. Note that the plasma is centred about a major radius R_o~3.0m, and the major radius of the limiter is at R=4.17m. These profiles have been truncated at R=4m (R=3.9m for the 1MA case) because of the large uncertainties in diagnostic measurements in the plasma edge region. In general, the effective resistivity derived from equilibrium analysis is in better agreement with the neoclassical value than

the Spitzer value derived from temperature profiles. However, the diagnostic uncertainties are such that Spitzer resistivity cannot be conclusively eliminated (particularly in view of the uncertainty in the profile of Z_{eff}). Nevertheless, this conclusion is consistent with the results of a global analysis of resistivity [15], which obtained good agreement between the volume average value of plasma resistivity derived from an analysis of current and loop-voltage measurements and the neoclassical value (rather than the Spitzer value).

3. ROLE OF MHD INSTABILITIES IN CURRENT PENETRATION

3.1 Type of Instabilities Predicted for the Current Rise

To investigate the relationship between the observed mhd activity and the processes affecting current penetration, we have analysed the evolution of typical discharges in the parameter plane (q_o, q_a) [16]. By drawing the boundaries of various mhd instability regions, obtained from the model of [13], in this plane, it is possible to interpret current penetration processes. Briefly, this is a cylindrical model in circular geometry which uses a simplified current profile of the form

$$j(r) = j_o \, (1 - (r/a)^2)^{\nu} \qquad (12)$$

where $\nu = q_a/q_o - 1$, to deduce a number of simple criteria necessary for the occurrence of certain classes of mhd instabilities. While the model, and the criteria derived from it, contain significant simplifications, there is remarkable agreement between the behaviour of discharges which one might expect on the basis of this analysis, and our experimental observations (as will be discussed in succeeding sections). In particular, if the trajectory of a discharge is plotted in the (q_o,q_a) plane, one can identify regions of this plane where the conditions necessary for the appearance of certain instabilities are fulfilled. This is done in figure 4, where several time points from the trajectories followed by a sample of JET pulses are plotted. One remarkable aspect of this plot is the fact that relatively few points lie in the 'stable' region.

For clarity we discuss the trajectory of a particular pulse (2214) which, as shown in figure 5, passed through all regions of the plane. Identification of the times of interest which are labelled in the figure can

be obtained from the plasma current trace in figure 1. Detailed magnetic equilibrium calculations show that the current profile initially exhibits a significant skin effect, and that it becomes gradually more peaked as the trajectory reaches the equilibrium state. It is also found that the trajectory reaches q_o~1 at approximately the same time as sawteeth appear, and that it remains in this condition during a substantial period of the current decay. Thus, there is qualitative agreement between the form of the j (and q) profiles at various times and the region in which the trajectory lies.

This relationship between the j profiles and the regions of the (q_o, q_a) plane is further illustrated by the two other cases shown in figure 5. These trajectories show very distinct patterns of evolution. Pulse 2442 starts in the 'double tearing' sector($q_a < q_o$) and then remains entirely in the 'kink' sector($q_o < q_a < 2q_o$) before disrupting during the flat top. The current density profile starts hollow and peaks 3s after breakdown, the trajectory then being in the 'kink' region. This is in contrast to pulse 2214 which has a similar slow rise, but enters the 'kink' region earlier and also becomes fully peaked earlier (after 2s), terminating within the 'tearing-internal' band($1 < q_o < 3$). The third example (shot 2044) is rather unusual, but interesting, because it always has a peaked current profile and, as expected, it crosses only the 'tearing' region. Figure 6 summarises the evolution of the current j(r) and q(r) profiles for the pulses 2214, 2442 and 2044, obtained from the equilibrium codes.

3.2 Current Redistribution by Magnetic Relaxation

The trajectories described here show a significant correlation with the spectra of mhd activity observed. Figure 7 shows the magnetic activity, signal plotted as a function of the safety factor q_a, for the three pulses shown in figure 5. A study of the current rise phase for many pulses reveals that trajectories lying in the 'double-tearing' or 'kink' regions exhibit mhd actvity spectra of the form seen for pulse 2442, i.e. with distinct peaks close to rational values of q_a, that is $q_a = m/n$ with $n = 1$ or, sometimes, $n = 2$. Evidence for the redistribution of j for pulses such as 2442 and 2431 with similar trajectories, is shown in the plot of ℓ_i versus q_a (figures 8a,b), where discontinuous changes in ℓ_i at integral values of q_a are seen.

On the other hand, trajectories which have crossed into the 'tearing' region have mhd spectra which generally show less structure, with peaks of

the signal often uncorrelated to integral values of q_a (for example pulse 2044 which remains for the most part in the 'tearing'region, has a broad mhd spectrum). The same is true for the evolution of ℓ_i.

3.3 Influence of Current and Density Ramp Rates

Experimentally it is found that the trajectory of the initial phase depends on the operating conditions. For example, 2214 and 2442 have the same slow current ramp rates, but pulse 2442 has higher current and density ramp rates during the fast rise phase (figures 9a,b). A convenient representation of the input conditions is given by the Hugill diagram ($1/q_{cyl}$, $\bar{n}R/B_T$). Figure 9c shows the Hugill trajectories for shots 2214 and 2442. The fact that pulse 2214 crosses into the 'tearing' region may be associated with the lower ramp rate in the Hugill diagram. The Hugill trajectories for a larger set of pulses shown in figure 10 indicate that above a certain Murakami parameter value for the fast current rise and below a certain ramp rate for the slow current rise the (q_o,q_a) trajectories tend to separate into the 'kink' and 'tearing' types. Most disruptions during the current rise occur in the 'kink' region.

Although the different regions in the (q_o,q_a) plane seem to determine the type of mhd instabilities observed, it should be stressed that being in a particular region is not a sufficient condition for such activity to occur. It is found experimentally that the level of mhd activity is also determined by operating conditions. Favourable conditions for occurrence of the 'kink' type instabilities during the fast current rise are produced by the increase of the current ramp rate (the dependence on other parameters is discussed in [17] and [18]). Figure 11 shows a sequence of shots in which the current and density ramp rates during the fast current rise were varied. Note that in pulse 2445, the current ramp rate was significantly lower during the period 0.2-1.0s than for the other pulses shown. This appears to have significantly reduced the mhd activity during this phase, in spite of the fact that all four pulses shown have very similar trajectories in the (q_o,q_a) plane up to 1s.

4. SUPERPOSITION OF A CURRENT RAMP DURING THE FLAT TOP

A series of experiments was performed in which the plasma current was

programmed to rise from one flat top level of 1MA to a second flat top level of 2MA [15]. During this current rise phase, lasting 2 seconds, the plasma shape was approximately constant. Parallel resistivity was studied both during the current rise and during the subsequent penetration phase at 2MA. The internal inductance ℓ_i calculated for these equilibria falls from 1.6 to 1.05 during the current rise as shown for shot 4896 in figure 12a. Approximately 1.4 seconds after the end of the rise phase the current is fully penetrated and ℓ_i has increased to its final value of 1.25. The period of 1.4 seconds is marked in figure 12b as the time taken for the loop voltage on the plasma surface to approach the loop voltage on axis. Figure 13 shows the ratios η_{eff}/η_s and η_{eff}/η_* against major radius at a particular time (t=7s) during the current rise. The vertical bars indicate the spread of values in time at a particular major radius.

The resistivity inferred from ECE or determined from mhd equilibria is, within a factor 0.85-1.15, equal to the neoclassical value given by [14] and higher, by a factor 1.4-2.6, than the Spitzer value given by [19]. This strengthens the conclusion that resistivity in JET is close to neoclassical even during the ramp. This result should be compared with a Doublet III study [8] in which trapping was found to be far less dominant.

5. CONCLUSIONS

A detailed study of plasma resistivity in JET has shown that during the plasma 'flat-top', and at times when the current profile is changing slowly, the resistivity is well described by neoclassical theory. As a result, current penetration occurs on a timescale consistent with neoclassical diffusion rates. This applies equally to plasmas in quasi-steady state conditions, and plasmas with applied external electric fields. Note that although the neoclassical rather than Spitzer values appear to be a better description of plasma resistivity in JET, experimental errors are such that Spitzer resistivity cannot be completely excluded.

During the current rise phase, however, current penetration is substantially more rapid than expected from a resistive diffusion calculation. It appears, therefore, that the rate at which current penetrates is enhanced by the experimentally observed mhd activity (as has been observed in earlier experiments). We have therefore attempted to analyse the formation of the current and temperature profiles in terms of the mhd stability properties of the plasma. Our conclusion is that the

evolution of current and temperature profiles in JET may be understood in terms of the trajectory of the discharge in the (q_o, q_a) plane. It is found that the plasma evolves through regions in this plane which are predicted to be mhd unstable. While substantial mhd activity is observed, which is correlated with rapid current penetration, the occurrence of such mhd instabilities generally has no deleterious effect on the flat-top performance. As the mhd activity decays, current penetration approaches the neoclassical value, and becomes neoclassical as the current plateau value is reached. Generally the plasma current flat-top is reached with $q_o \sim 1$, and this state is maintained into the decay phase.

ACKNOWLEDGEMENTS

It is a pleasure to acknowledge our colleagues in the JET Team who have operated the tokamak and its associated diagnostics during the experiments reported here.

REFERENCES

[1] Blum, J., Thooris, B. and Le Foll, J., 'Parametric identification of the plasma current density from the magnetic measurements and pressure profile', JET Contract JT3/9008 (198).

[2] Christiansen, J.P., 'Integrated Analysis of Data from JET', JET Report JET-R(86)04 (1986).

[3] Costley, A.E., Baker, E.A.M., Brusati, M., Bartlett, D.V., Campbell, D.J. et al., Controlled Fusion and Plasma Physics (Proc. 12th Europ. Conf., Budapest, 1985), 9F-I, (1985) 227.

[4] Mirnov, S.V., Nucl. Fus. 9, (1969) 57.

[5] Hutchinson, I.H., Morton, A.H., Nucl. Fus. 16, (1976) 467.

[6] Granetz, R.S., Hutchinson, I.H., Overskei, D.O., Nucl. Fus. 19, (1979) 1587.

[7] Hawryluk, R.J., Bol, K., Johnson, D., Nucl. Fus. 19, (1979) 1519.

[8] Stambaugh, R.D., Blau, F.P., Ejima, S., Jahns, G.L., Luxon, J.L., Shimada, M., Taylor, T.S., Waltz, R.E., Nucl. Fusion 22, (1982) 395.

[9] Karger, K., Klueber, O., Niedermeyer, H., Schueller, F.C., Thomas, P.R., in Controlled Fusion and Plasma Physics (Proc. 11th Europ. Conf., Aachen, 1983).

[10] Meyerhofer, D.D., Goldstone, R.J., Kaita, R., Cavallo, A., Grek, B., Johnson, D., McCone, D.C., McGuire, K., White, R.B., Nucl. Fus. 25, (1985) 321.

[11] Furth, H.P., Rutherford, P.H., Selberg, H., Phys. Fluids 16, (1973) 1054.

[12] Stix, T.H., Phys. Rev. Lett. 36, (1976) 521.

[13] Wesson, J.A., Nucl. Fus. 18, (1978) 87

[14] Hirschman, S.P., Sigmar, D.J., Nucl. Fus. 9, (1981) 1077

[15] Christiansen, J.P., Campbell, D.J., Cordey, J.G., Ejima, S., Lazzaro, E., Contr. Fusion and Plasma Physics, (Proc. 12th Europ. Conf., Budapest, 1985), 9F-I (1985) 327.

[16] Lazzaro, E., Nave, M.F., 'Results of Magnetic Data Analysis of JET Current Evolution', JET-DN-T(85)24 (1985).

[17] Notkin, G.E., Fizika Plasmy 11 (1985) 62 (in Russian).

[18] Lomas, P., Kellman, A., Lazzaro, E., Malacarne, M., Schüller, F.C., Piekaar, H.W., Thomas, P.R., Tanga, A., Bull. Am. Phys. Soc. (27th Annual Meeting of the Division of Plasma Physics of the American Physical Society, San Diego, 1985) 30 (1985) 1524.

[19] Hinton, F.L., Haseltine, R.D., Rev. Mod. Phys. 48(1976) 239.

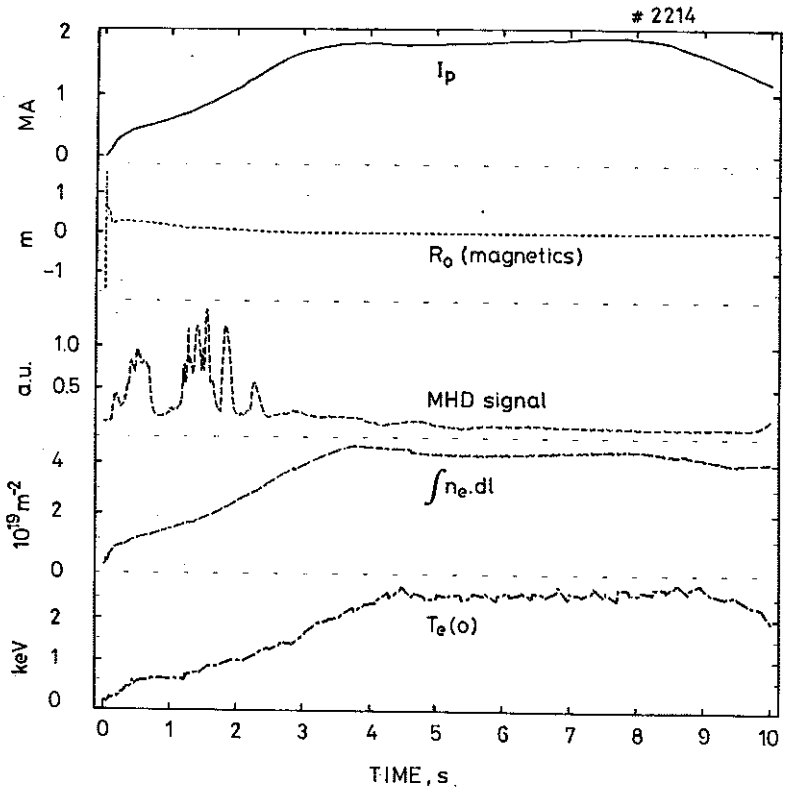

Fig. 1(a) Evolution of several principal parameters during a JET pulse: plasma current, I_p; magnetic axis, R_o; mhd activity signal; line integral of density, $\int n_e dl$; central electron temperature, $T_e(0)$.

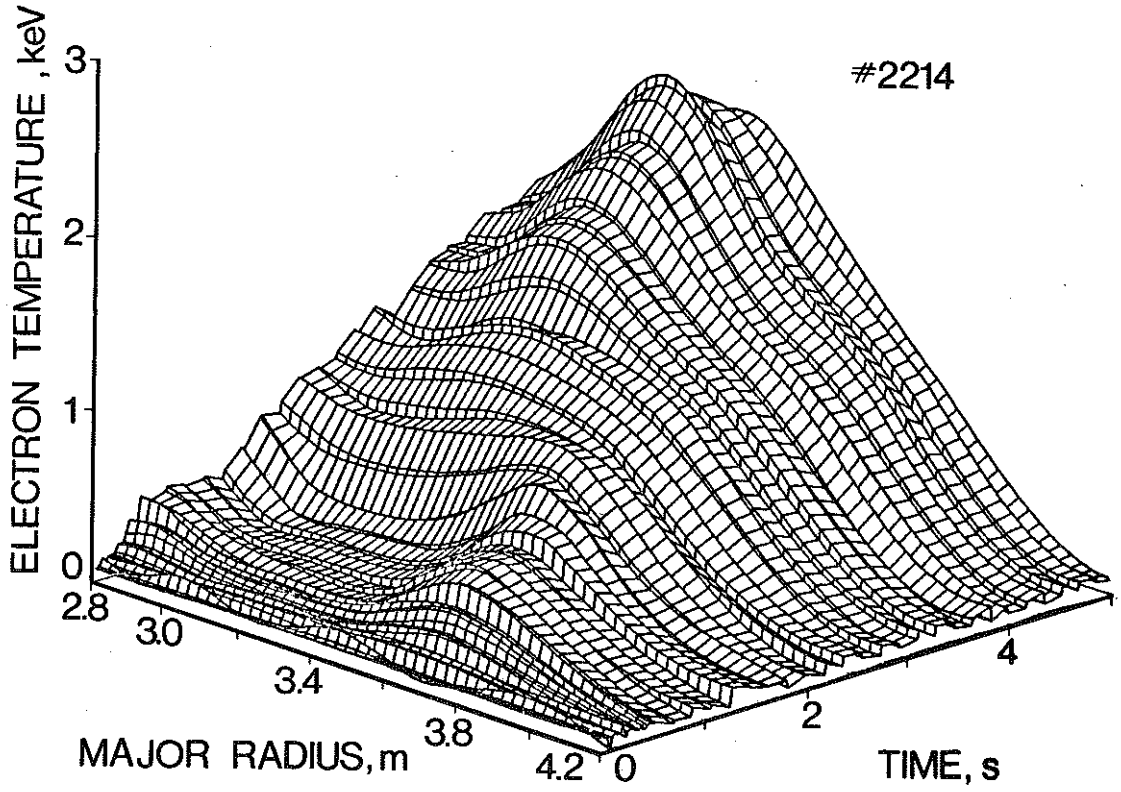

Fig. 1b Development of the electron temperature profile during the first 5s of this pulse. Note the evolution from the hollow profiles at early times to the peaked profiles which persist during the current flat-top.

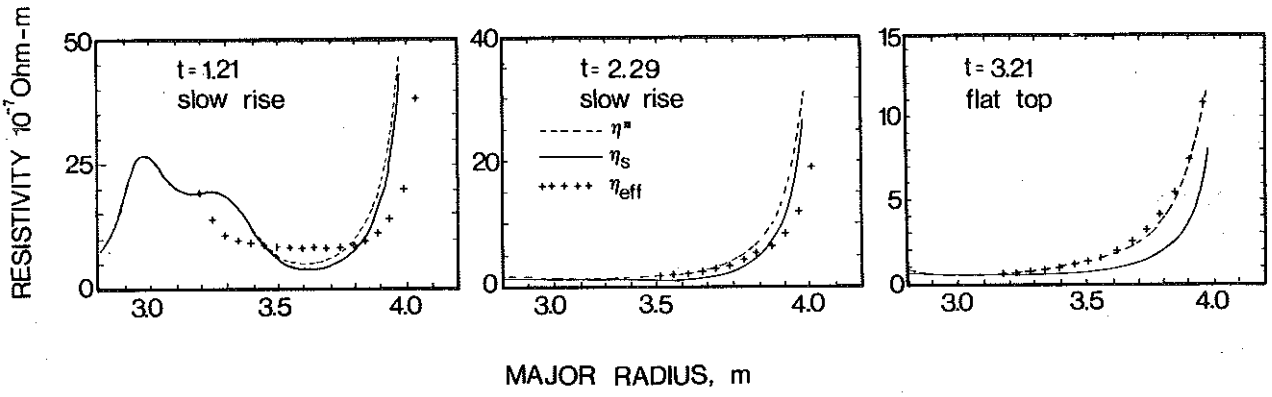

Fig. 2 Comparison of radial profiles of effective resistivity η_{eff} (crosses), neoclassical resistivity η^* (dashed line), and Spitzer resistivity η_s (full line) at three times during JET pulse 2214.

P(86)46

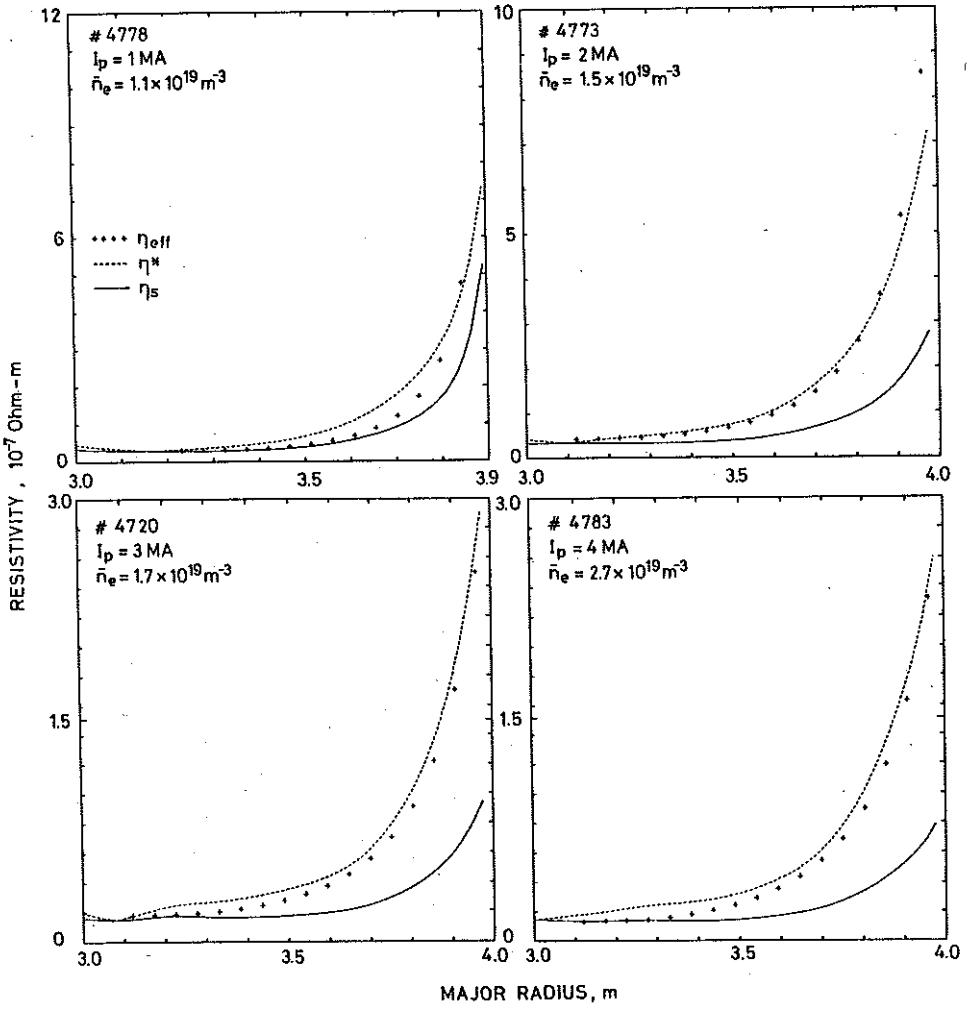

Fig. 3 Comparison of radial profiles of η_{eff}, η^* and η_s for a range of JET discharge parameters. $B_\phi = 3.44$ T in each case. These results are typical of the good agreement found between η_{eff} and η^* once the current flat-top is reached.

P(86)46

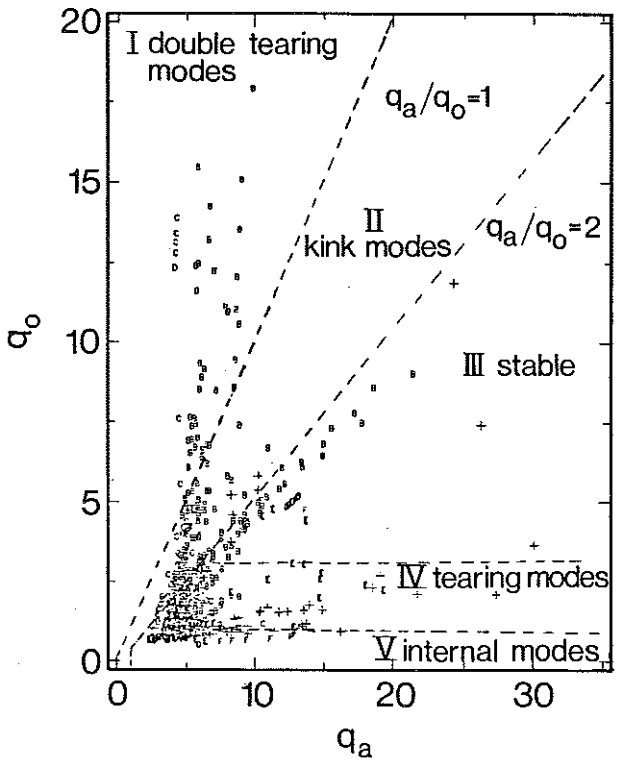

Fig. 4 Scatter plot of JET pulses in the plane (q_0, q_a). The stability boundaries for various forms of mhd activity (derived from [13]) are superposed.

P(86)46

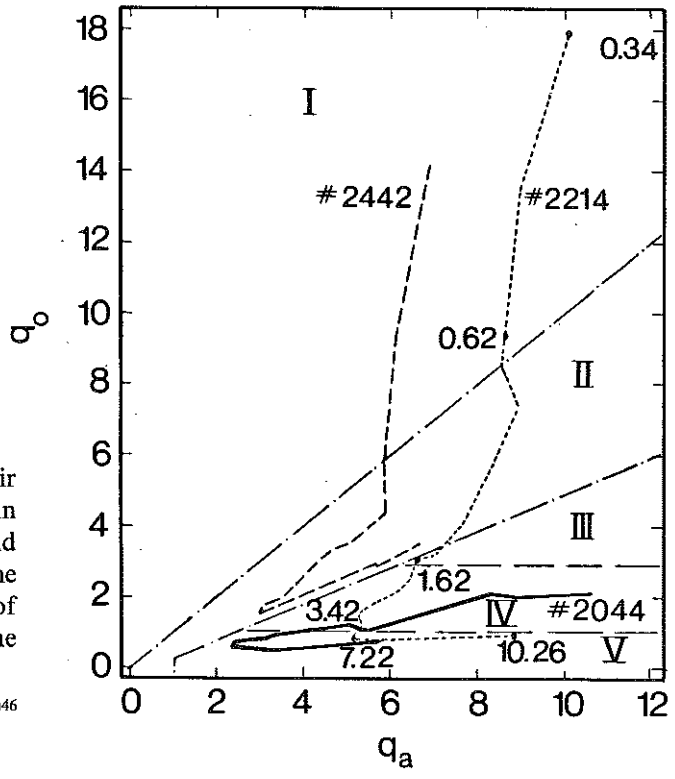

Fig. 5 Trajectories of 3 JET pulses during their evolution and decay. Several times of importance in the trajectory for pulse 2214 are indicated. It should be noted that t = 0.34 s corresponds to the end of the fast current rise, t = 3.42 s corresponds to the end of the slow current rise, t = 10.26 s corresponds to the end of the flat-top.

P(86)46

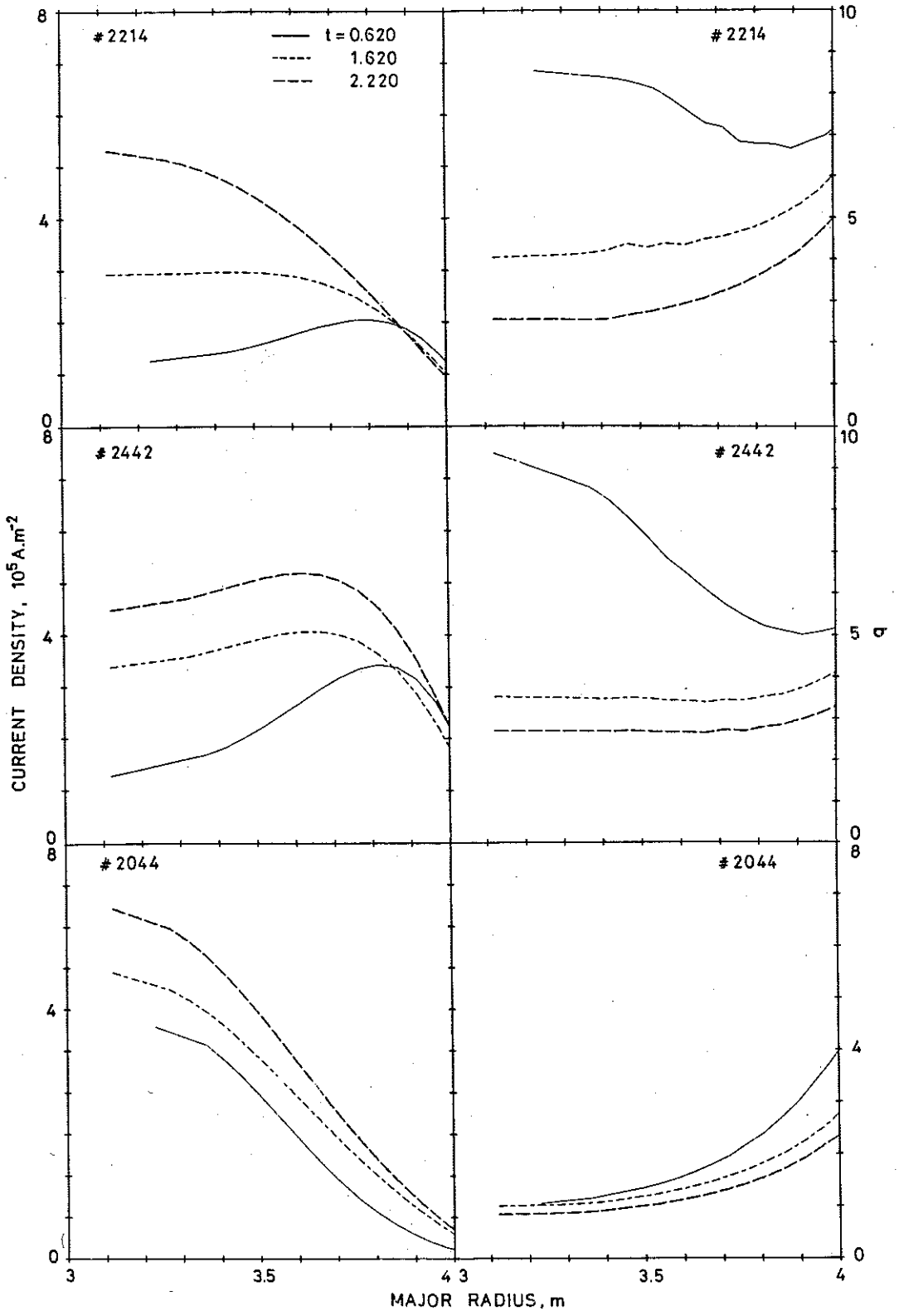

Fig. 6 Evolution of current j(r) and safety factor q(r) profiles for pulses 2214, 2442 and 2044, obtained from the magnetic equilibrium codes.

P(86)46

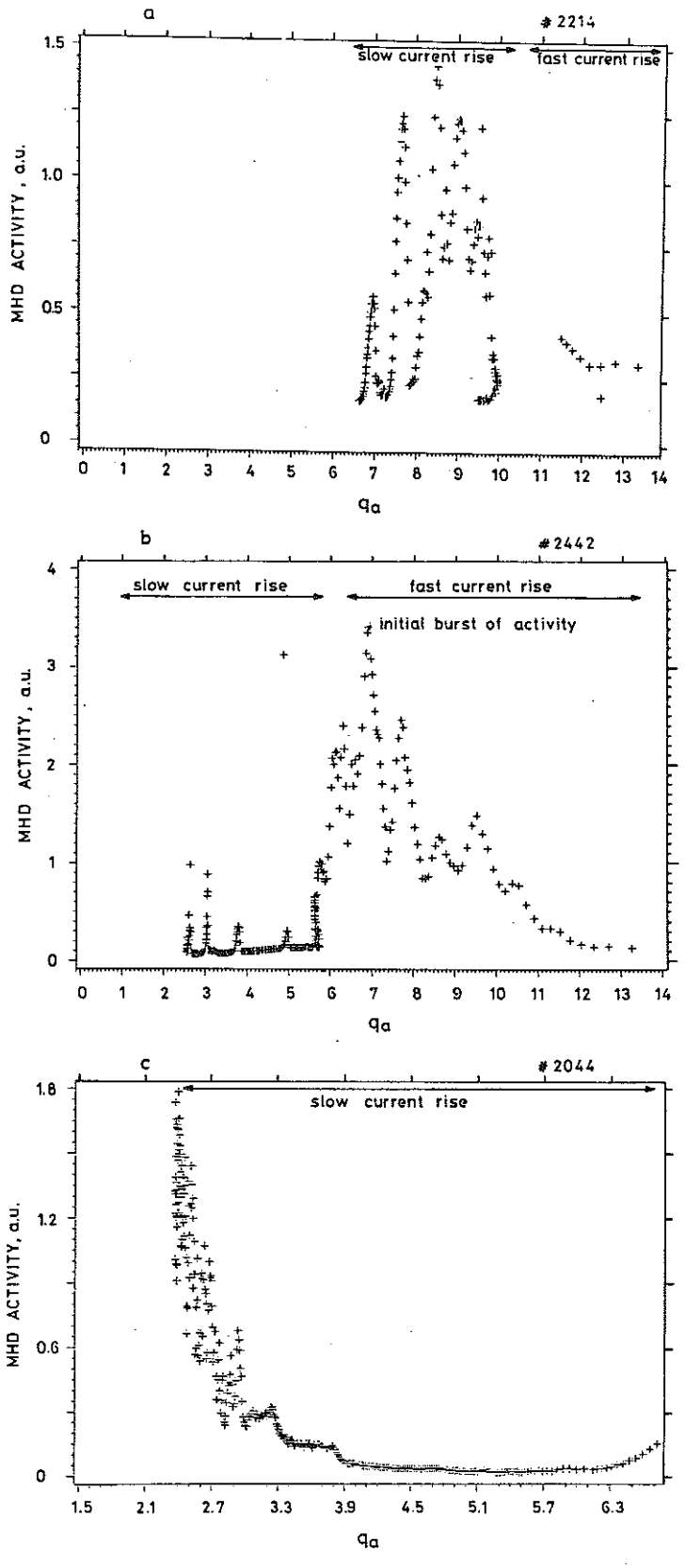

Fig. 7 mhd activity signal plotted against q_a for the three pulses shown in fig. 5.

P(86)46

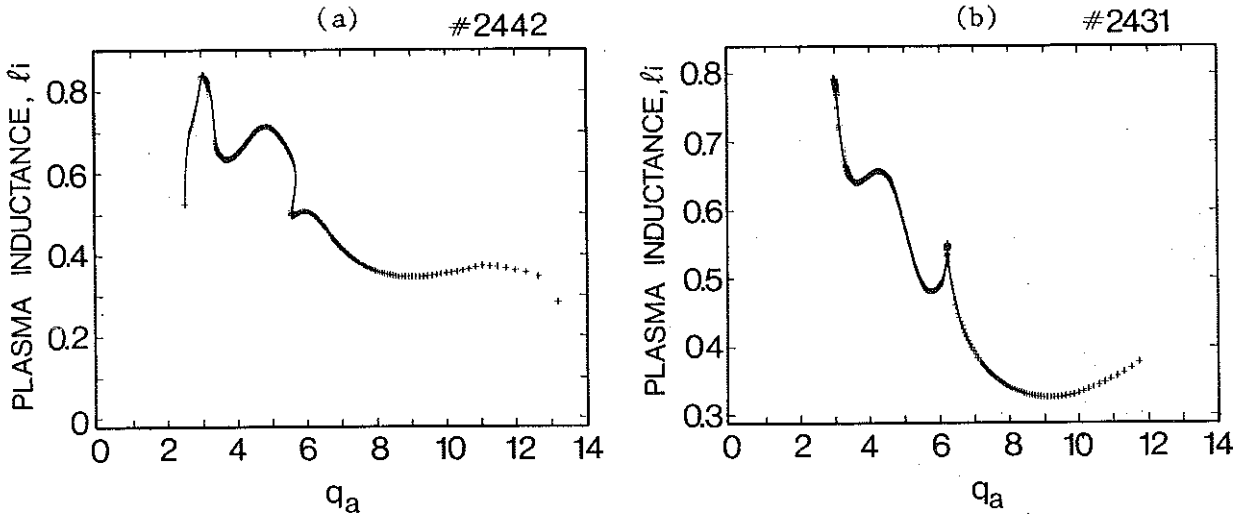

Fig. 8 ℓ_i plotted as a function of q_a for pulses 2442(a) and 2431(b); (both pulses have similar (q_o, q_a) trajectories and mhd spectra).

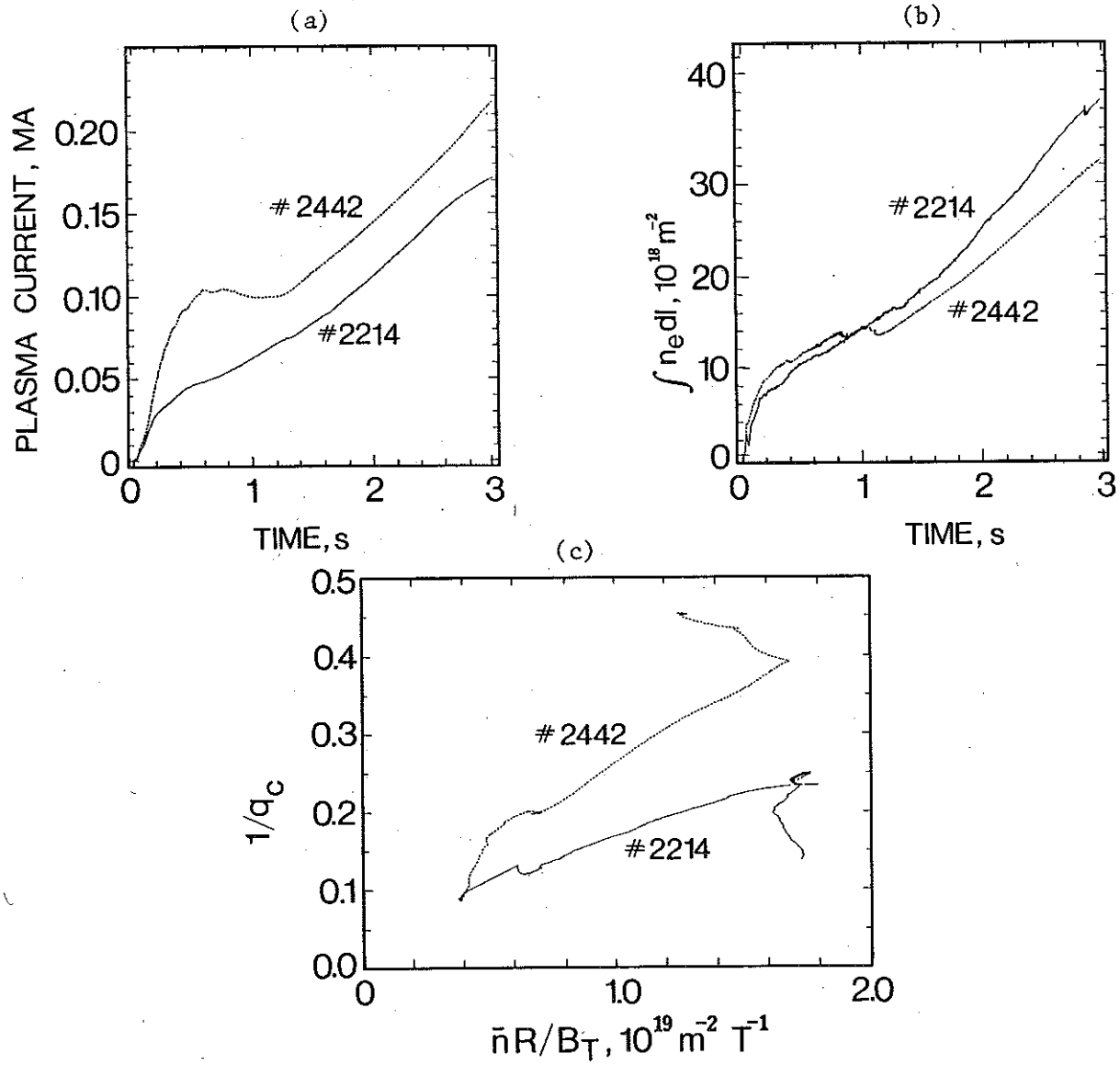

Fig. 9 Current ramp versus time (a) and line integral density versus time (b) for the current rise phase of shot 2214 and 2442. Corresponding trajectories in the Hugill diagram (c).

P(86)46

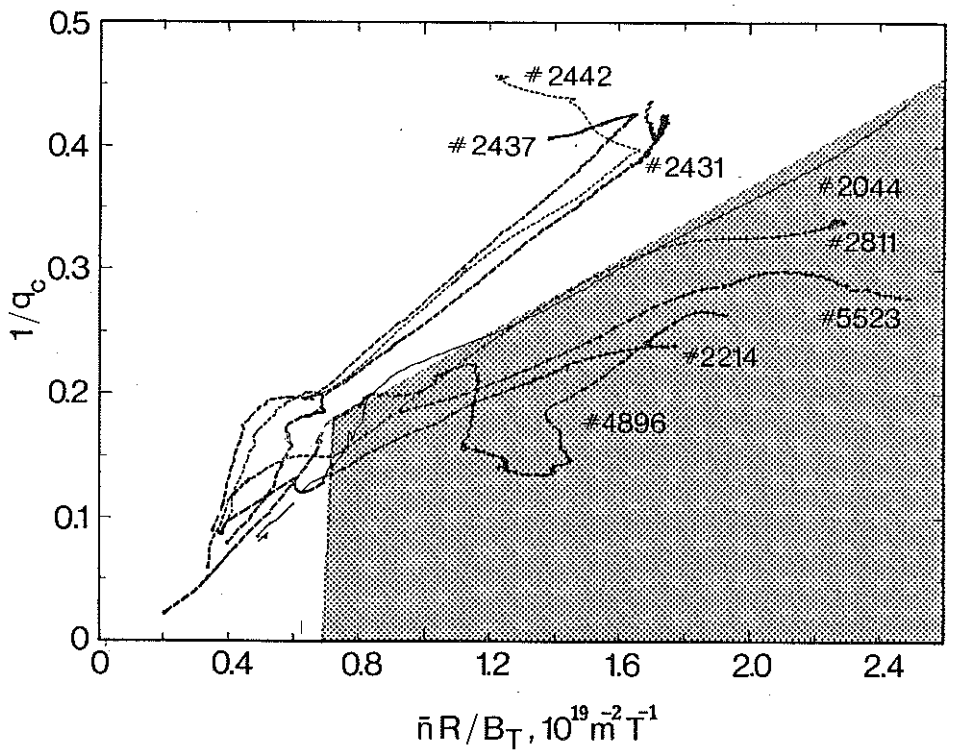

Fig. 10 Hugill trajectories for the current rise phases of several shots. The shaded region corresponds to the 'tearing' region in the (q_o, q_a) diagram .

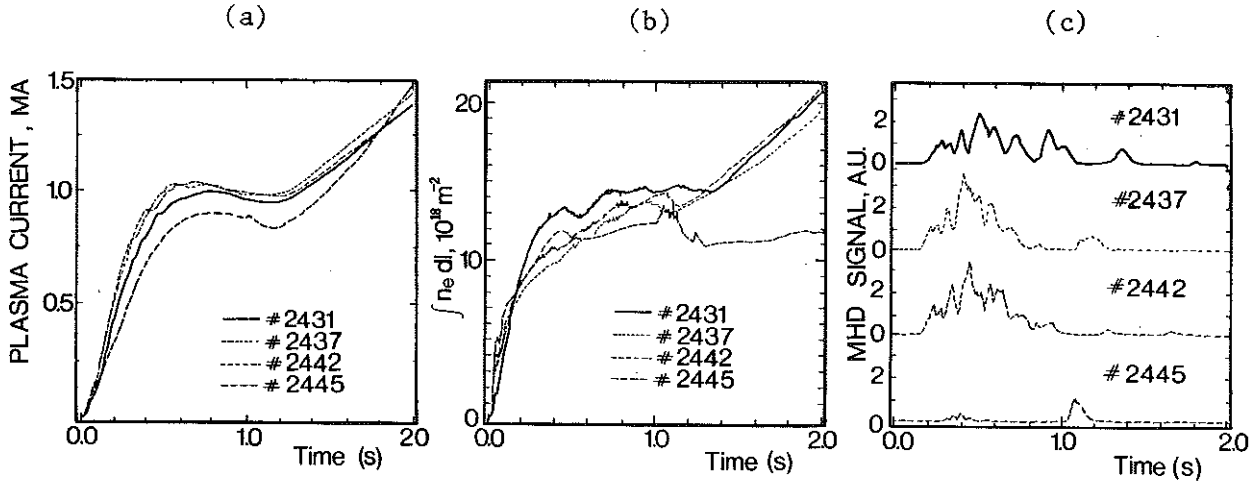

Fig. 11 Current ramp versus time (a), line integral density versus time (b) and mhd activity (c), for a sequence of shots in the 'kink' region.

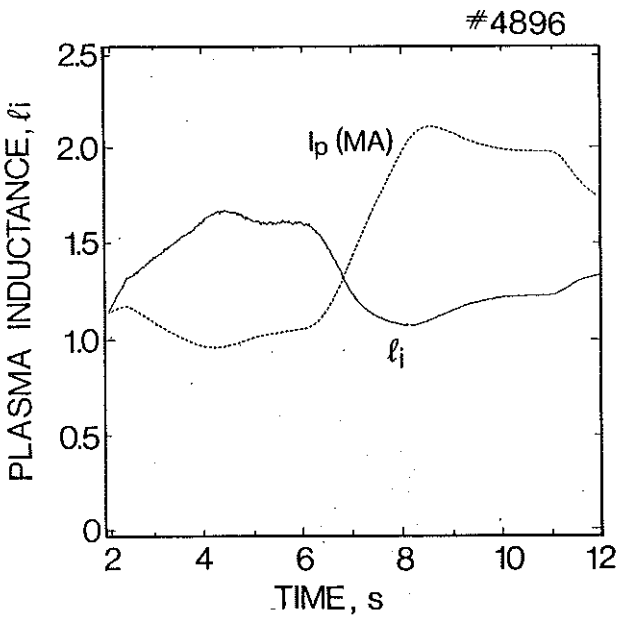

Fig. 12a Internal inductance ℓ_i and current in MA as a function of time for shot 4896.

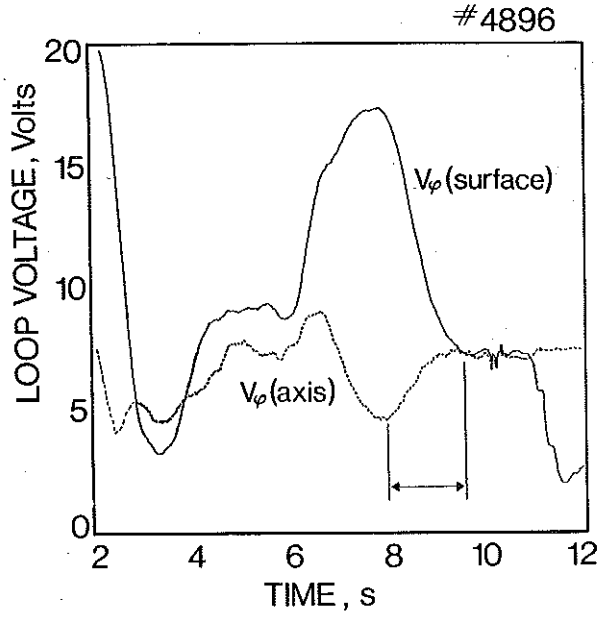

Fig. 12b Loop voltages on plasma surface (solid) and on axis (dashed line) versus time for shot 4896. The field penetration period at I=2MA is marked.

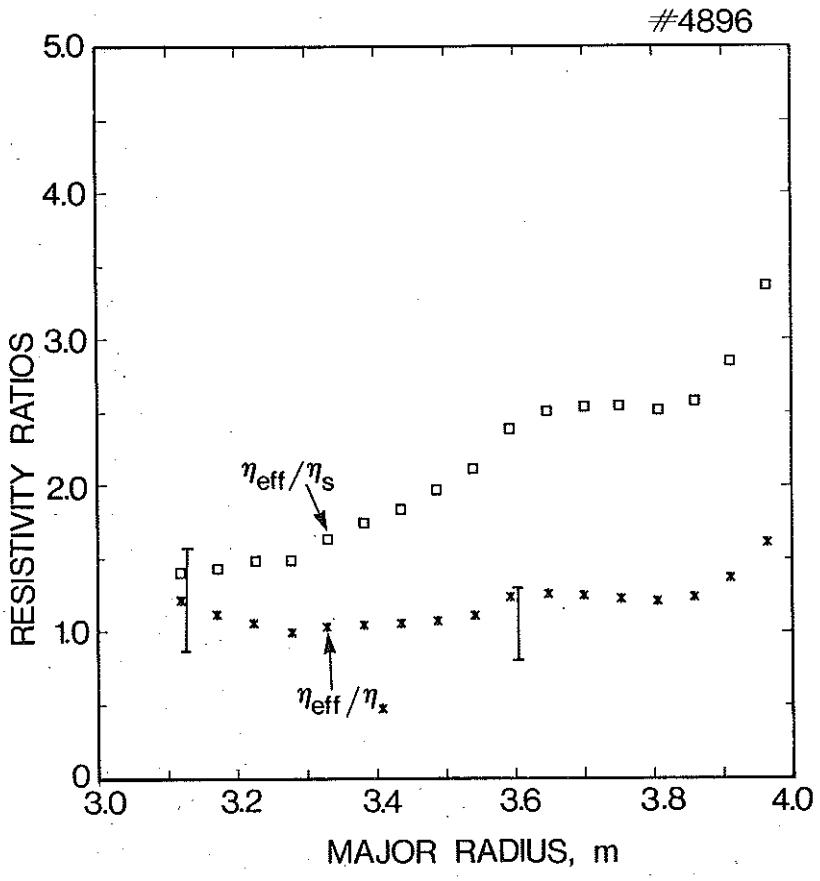

Fig. 13 The ratios η_{eff}/η_s and η_{eff}/η^* plotted versus R at t=7sec.

P(86)46